ATMOSPHERIC VISIBILITY MEASUREMENTS USING VIDEO CAMERAS: RELATIVE VISIBILITY

Taek Mu Kwon

Department of Electrical and Computer Engineering
University of Minnesota Duluth
CTS 04-03

Technical Report Documentation Page

1. Report No. CTS 04-03	2.	3. Recipients Accession No.	
4. Title and Subtitle Atmospheric Visibility Measurements Using Video Cameras: Relative Visibility		5. Report Date July 2004	
		6.	
7. Author(s) Taek Mu Kwon		8. Performing Organization Report No.	
9. Performing Organization Name and Address University of Minnesota Duluth Department of Electrical and Computer Engineering 1023 Unversity Drive Duluth, Minnesota 55812		10. Project/Task/Work Unit No.	
		11. Contract (C) or Grant (G) No.	
12. Sponsoring Organization Name and Address Minnesota Department of Transportation 395 John Ireland Boulevard Mail Stop 330 St. Paul, Minnesota 55155		13. Type of Report and Period Covered	
		14. Sponsoring Agency Code	
15. Supplementary Notes			

16. Abstract (Limit: 200 words)

Poor visibility conditions often lead to large-scale chain accidents causing human fatalities and property damage. Such visibility-related vehicle accidents could have been prevented if motorists were warned ahead of time to reduce speed and remain cautious before moving into the poor visibility zone. The objective of this research was to advance the visibility measurement technologies that compute visibility through processing images captured by video cameras.

There are two fundamental difficulties in measuring visibility. The first is that visibility is a complex multivariable function of many parameters such as objects available, light sources, light scatter, light absorption, etc., so that measurements of one or two parameters (as in most of today's visibility meters) cannot accurately estimate the true human-perceived visibility. On the other hand, any attempt to measure every possible atmospheric parameter to derive human perceived visibility is simply too complex and costly. The second source of difficulty is contributed by an attempt to express the spatially variant nature of atmospheric visibility using a single representative value, distance. It works only if the atmosphere is uniform, which rarely happens. A solution presented in this report is to measure visibility using visual properties of video images (perceived information) instead of indirectly measuring physical properties of atmosphere and converting them to visibility. The spatial variance problem in visibility was solved by introducing a new concept of relative measurement of visual information referred to as the Relative Visibility (RV).

This report also includes a study result on the limitation of CCD cameras in visibility measurement applications, and shows how to overcome them through spatially arranged multiple targets. In addition, we explored various apparatuses of Near Infrared (NIR) light source and cameras for measuring night visibility. This result is included in the report.

17. Document Analysis/Descriptors Atmospheric Visibility, Relative Visibility, Video Cameras, Near Infrared Light Source, Near Infrared Camera, Contrast Computation, Flat Road Model, MRV		18. Availability Statement No restrictions. Document available from: National Technical Information Services, Springfield, Virginia 22161	
19. Security Class (this report) Unclassified	20. Security Class (this page) Unclassified	21. No. of Pages 53	22. Price

ATMOSPHERIC VISIBILITY MEASUREMENTS USING VIDEO CAMERAS: RELATIVE VISIBILITY

Final Report

July 2004

Principal Investigator:
Taek Mu Kwon, Ph.D.
Department of Electrical and Computer Engineering
University of Minnesota Duluth

Center for Transportation Studies
University of Minnesota

CTS 04-03

Acknowledgements

The author would like to thank Ms. Roberta Dwyer of the Minnesota Department of Transportation (Mn/DOT) for her direct and indirect help provided throughout this project. Thanks to Mr. Edward Fleege for obtaining a visibility meter and helping the hardware set up for this visibility study before he retired from Mn/DOT. Thanks are also extended to the Center for Transportation Studies at the University of Minnesota, Twin Cities for providing the funds for this research. Mrs. Carol Wolosz of the Northland Advanced Transportation Research Laboratories patiently read the draft manuscript and corrected many typographical and grammatical errors. Thanks to Mrs. Carol Wolosz for kindly volunteering her time.

Executive Summary

Poor visibility conditions often lead to large-scale chain accidents causing human fatalities and property damage. Such visibility-related vehicle accidents could have been prevented if motorists were warned ahead of time to reduce speed and remain cautious before moving into the poor visibility zone. Poor visibility reduces the sight distance of motorists, such that if the traveling vehicle's stopping distance is longer than the motorist's sight distance, and if a stopped vehicle or an object is present outside the range of the sight distance, crashes are bound to occur. Such crash accidents can be easily avoided if the stopping distance is decreased to a range shorter than the sight distance by reducing the vehicle's traveling speed. Therefore, the challenge remains to accurately measure visibility in real time to determine the optimal speed limit and notify drivers of a safe speed limit in real time. The objective of this research was to advance visibility measurement technologies that work based on processing images captured through video cameras.

There are two fundamental problems in converting atmospheric parameters into visibility, which is the case in most of today's visibility meters. The first is that visibility is a complex multivariable function of many atmospheric parameters such as air light[1], objects available, light scatter, light absorption, etc., so that measurements of one or two parameters (as in most of today's visibility meters) cannot accurately estimate the true human-perceived visibility. On the other hand, any attempt to measure every possible atmospheric parameter to derive human perceived visibility is simply too complex and costly. The second source of difficulty is contributed by an attempt to express the spatially variant nature of atmospheric visibility using a single representative value, distance. It works only if the atmosphere is uniform, which rarely happens. A solution presented in this report is to measure visibility using visual properties of video images (perceived information) instead of indirectly measuring physical properties of atmosphere and converting them into visibility. The spatial variance problem in visibility was solved by introducing a new concept of relative measurement of visual information referred to as the Relative Visibility (RV).

This report also includes extensions of the first phase of the video-based visibility study [11] in which fixed multiple targets were used. Theoretical analysis and verification using real examples on limitations of using a small number of visibility targets are presented in this report. The main finding was that the accuracy of visibility measurements increases as more targets at varying distances are available. For night visibility, this report includes the results of a feasibility study on utilizing apparatuses of low cost, near infrared (NIR) light sources and cameras. It was found that measurements of air-opacity using a reflective NIR source from specific types of surface properties provided the most accurate representation of night visibility. The rest of the report is focused on introducing the RV concept and theory, and development of image-processing techniques for computing RV.

[1] The amount of light intensity in the visible spectrum available in the measuring space.

TABLE OF CONTENTS

LIST OF FIGURES

LIST OF TABLES

CHAPTER 1: INTRODUCTION

1.1 Nature of Visibility

Atmospheric visibility can be reduced by fog, snow, dust, sand, smog or any combination of them, and is a part of normal atmospheric phenomena. Although the accuracy of weather forecasting has steadily improved over the years, accurately predicting visibility conditions is considered extremely difficult. The difficulty lies in that reduced visibility frequently occurs in localized areas as a result of microclimate changes in that region, and in many cases the condition changes in a matter of minutes or seconds. Such visibility changes along highways can be fatal causing large-scale pileup accidents involving many vehicles. In the western part of Minnesota, severely reduced visibility by blowing snow on highways is a well-known problem that creates extremely difficult and dangerous driving conditions. The Minnesota Department of Transportation (Mn/DOT) often resorts to closing the highways to avoid deadly crash and rollover accidents if severely reduced visibility is reported.

Although reduced visibility along highways presents a great danger to motorists, there exists a simple solution for avoiding crash accidents. Poor visibility reduces the sight distance of motorists up to the point at which motorists cannot see objects beyond the distance determined by visibility. Crash accidents occur because motorists cannot bring their vehicles to a stop or to a slow enough speed due to insufficient reaction time and braking distance after recognition of another vehicle or an object. This means that, if the vehicle was traveling at a speed that gives sufficient reaction and braking time for a complete stop within the sight distance, collisions can be avoided. Such a safe driving speed along with a safe following distance can be readily computed by combining the braking distance, sight distance, and reaction time if we know the visibility in real time [11]. Therefore, a solution for avoiding crash accidents under poor visibility is simply communicating a safe driving speed and following distance to motorists in real time. Advising motorists of driving speed in real time could be accomplished using variable message signs (VMS), but the challenge lies in accurately measuring visibility. The goal of this project is advancing the visibility measurement technology.

1.2 Visibility Definitions

According to the American Meteorological Society's Glossary [1], daytime atmospheric visibility is defined as the greatest distance from an observer where a prominent dark object against the sky at the horizon can be seen and identified by an unaided eye. At night, a known, preferably unfocused, moderately intense light source is placed as the visibility target of recognition for the measurement of maximum visible distance. These original visibility definitions were developed based on human observation of atmospheric visibility conditions. Although, these measurement definitions do not seem complicated, they present difficulties in scientific measurements

due to a number of ambiguities. The size and shape of the target, the light intensities for night targets, the air light intensities of the observing area, the observer's angle to the target and height, etc., have not been clearly defined while they significantly affect the measurements. More importantly, the requirement that visibility targets be both detected and recognized by the naked eye adds human factors. These ambiguities were significantly reduced, since Middleton's suggestion of the term "visual range," which was defined for daytime as a subjective estimate of atmospheric attenuation of contrast, and for nighttime as the attenuation of flux density [2]. In the Middleton's definition of visual range [2], the recognition portion of visibility was omitted, from which observer's visual acuity and judgments are no longer the factor. Further narrow definitions of visual ranges were introduced to limit the scope to specific applications, such as runway visual range, slant visual range, meteorological visual range, etc. [3]. Today, the terms "visibility" and "visual range" are almost interchangeably used without clear distinction suggested by Middleton. In the recent Federal Meteorological Handbook No. 1 published by the National Weather Service, the term visibility is still in use and defined as a measurement of the opacity of the atmosphere, and the handbook suggests observation of four different visibilities, i.e., prevailing visibility, sector visibility, surface visibility, and tower visibility [5].

Visibility study in this project is intended for surface transportation applications. As a result, we are more interested in the perceived maximum distance at which motorists can recognize vehicles and road boundaries than the measurement of atmospheric parameters. Therefore, the term, visibility, in this report more closely follows the original definition in [1] that was defined based on human perception. However, measuring human perceived visibility is extremely challenging, as discussed in the next section.

1.3 Background on Visibility Technologies

Many instrumentation approaches for measuring visibility have been developed over the years [2,3], but they can be said to fall into one of the following two categories: telephoto meters that measure luminance or flux from projectors, and light-scatter sensors that measure the amount of light scatter at a certain angle. Other instrumentation methods such as the optical counting of atmospheric particles [6-9] and image processing of digitized video images [11] have been developed, but they are only experimental study results and no commercialized products are available. Today's commercial products are predominantly based on measuring the amount of modulated lights scattered at a certain angle (forward scatter, back scatter, or side scatter) [10, 12], perhaps due to their compact and low cost designs. Although this method works fairly well under foggy conditions, its accuracy tends to significantly drop under snowy and rainy conditions [12]. This is due to space-variant light-scatter coefficients and non-uniform atmospheric densities that are more prevalent under snowy and rainy conditions. Consequently, such differences result in a measurement value that significantly differs from the visibility a human observer perceives. To date, manual measurements by human subjects using appropriately designed targets are considered to be most accurate and reliable, despite many visibility-measurement methods have been developed over the years.

Measurements of visibility mentioned above can be said to belong to a class of absolute measurements that must produce an absolute value, i.e., distance, as the end result. Unfortunately, absolute visibility measurements computed from atmospheric parameters cannot accurately estimate what human observers perceive. There are two factors that cause the differences. The first is that visibility is a complex value that is influenced by many factors such as air light, objects available, light scatter, light absorption, etc., and the measurements of only one or two factors are not sufficient to accurately estimate the human perceived visibility. On the other hand, any attempt to measure every possible atmospheric factors to derive human perceived visibility is simply too complex and costly. The second source of difference is contributed by an attempt to express the spatially variant nature of atmospheric visibility using a single representative value, distance. It may work only if the atmosphere is uniform, which rarely happens. A solution presented in this report and the first phase of this research [11] is to understand visibility using visual properties such as acuity of objects in the varying distance instead of physical atmospheric properties. Video-based approaches provide an important intrinsic advantage over the light-scatter or other atmospheric coefficients based approaches; the image acquisition processes between the camera lens system and the human eye are similar. A video image-based approach along with multiple targets was studied in the first phase of this research [11] and this report presents the second phase of the study that further extends the video-based approach.

1.4 Relativity in Visibility

While using video images simplifies visibility measurement by not directly dealing with various atmospheric effects, it still presents a difficult challenge when an absolute measurement is to be derived from the image. Visibility at any given time is spatially variant and cannot be effectively represented by a single value. Statistical measurements such as an average can mislead the spatially variant conditions. As a solution for this spatial variant problem, this research introduces a completely new concept based on a relative measurement of visibility. To illustrate the reasoning, consider two images taken from the same location under two different visibility conditions as shown in Figure 1. We can readily tell that image (a) has worse visibility than (b). To be more accurate, we just need to determine how much the visibility in image (a) is worse than (b), which can be more effectively computed using image-processing techniques. Image (b) was taken on an ideal clear day that provides the best visual information so that it can be used as a reference. An interesting observation is that spatial variance of visibility is reduced to loss of visual information from an ideal condition. Suppose that after some image processing we found that the visibility condition in (a) has 30% less visual information than the ideal visibility condition in (b). This is clearly a relative measurement based on visual information, which is important to real world applications such as driving. By generalizing this example, Relative Visibility (RV) is introduced as a percent of visual information available in reference to an ideal visual condition in the area of measurements. From this relative visibility, safe speed limits could be more accurately established, since motorists maneuver vehicles mostly based on visual information.

In this report, we focus on developing a concrete concept and measurement approaches for RVs in highway applications. However, the same principle could be easily extended to other visibility applications. For the representation of relativity, we adopt a normalized expression where relative visibility is represented by a real number between zero and one, so that it can be equivalently represented by a percent similarly to the representation of relative humidity. One of the gains of using RV in instrumentation is that video cameras, which are considered not effective in measuring atmospheric parameters, can become an effective tool. In addition, visual images provide an opportunity to verify whether the computation is correct or not through a manual inspection.

Figure 1: Comparison of visibility conditions through recorded images at the same location

CHAPTER 2: SYSTEM SETUP AND DATA COLLECTION

2.1 System Setup

For this study, a field laboratory station was set up at the Thompson Hill site located near Spirit Mountain along Interstate highway I-35 northbound, Duluth, Minnesota and its location is shown in the map in Figure 2.a. This is a well-known location in this region for visibility problems caused by lake effect fog and snow. Figure 2.b shows a picture taken in the direction of North from the site. The experimental setup includes targets (Figure 2.c), cameras mounted on a pole (Figure 2.d), and a cabinet that houses a PC and a frame grabber (Figure 2.e). Two cameras were mounted on the pole as shown in Figure 2.d: the camera at the top of the pole is a Charge Coupled Devise (CCD) color camera that captures images within visual spectrum and the camera at the bottom is a near infrared (NIR) camera with an NIR light source that captures images in the NIR spectrum region. Six visibility targets were installed at 20m, 40m, 100m, 150m, 200m, and 300m apart from the camera pole with increasing sizes according to the camera's perspective view affected by the camera's focal length. The targets at 20m and 40m were designed by embedding a constant light source to study night visibility.

2.2 Data Collection

Data collection was performed using a PC housed in the cabinet (Figure 2.e). In order to collect images from poor visibility ranges, a light scatter meter built by Bristol Industrial and Research Associate Ltd was installed at the 40m target. This sensor is called a HSS™ sensor (model number VPF-710) and generates extinction coefficients as the output and its installation on the target is shown in Figure 3. The extinction coefficients were translated into meters and used in visibility data collection and for comparative studies. Images were automatically collected through an algorithm based on the flow chart shown in Figure 4. The data collection algorithm works as follows. Images are captured at every 3 minutes and then evaluated to determine whether the image is worthwhile to save into the data collection folder or not. If the visibility was less than 1,000 meters and has been changed sufficiently enough to give variations in the image, the image file was saved into a data collection folder. To save the memory space, all images were saved in JPEG compression format. For the detailed data collection algorithm, please refer to Figure 4. The test data was collected for two years, 2000 and 2001.

Figure 2: Visibility study site at the Thompson Hill, Minnesota. (a) Top left: map of the site, (b) Top right: overall view, (c) Middle left: six visibility targets, (d) Middle right: camera pole, (e) Bottom left: cabinet houses a PC.

Figure 3: HSS™ (Model VPF-710) sensor integration at the 40m target.

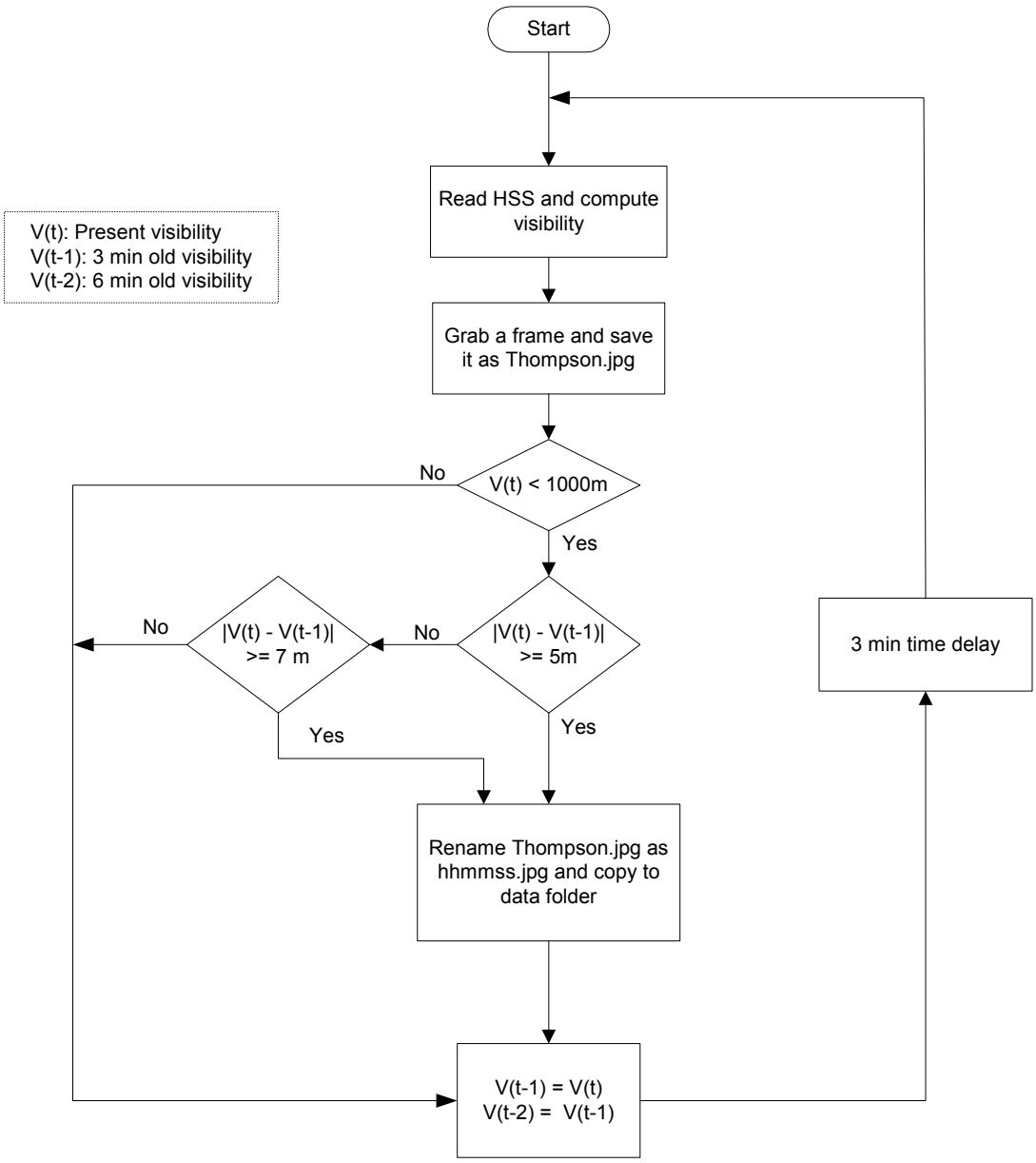

Figure 4: Flowchart for image data-collection algorithm

CHAPTER 3: VIDEO CAMERA LIMITATIONS ON LUMINANCE MEASUREMENTS, AND STUDY ON ACCURACY OF VISIBILITY MEASUREMENTS AFFECTED BY NUMBER OF TARGETS

3.1 Video Camera Analysis

Before developing visibility measurement algorithms using video images, it is important to understand the limitations of video cameras. In particular, the dynamic range of sampled pixels produced by video cameras is of prime importance for computing visibility because luminance differences generate contrasts in which objects are recognized. The question to ask is with what detail a video camera can distinguish gray scale (achromatic color). In order to test the gray scale of optical inspection systems and cameras, the Electronics Industry Association (EIA) devised a test pattern called EIA Equal Steps Density pattern or EIA 20:1. This standard pattern uses a principle that linear halftone density with fine pitch has logarithmic transmission, i.e., ultra fine halftone patterns with equal steps produce logarithmic gray levels. The standard EIA Gray Scale pattern has 15 density steps and was used as a target to study limitations of CCD (Charge Coupled Device) video cameras in measuring luminance.

The target used for testing gray level performance of a CCD camera in this study is a 8.5”x11” mylar variable density target supplied by Edmund Industrial Optics®. The 15 density steps in this mylar film represent a density of 0.07 to 1.5 on two progressions from high to low and low to high. This corresponds to optical density increments of 0.10. The variation between density steps is linear, which leads to a logarithmic change in diffused reflectivity. Since logarithmic reflectivity progression offers both finer and coarser increments than a comparable linear chart, it is often preferable for optic system testing. The video camera used for testing was Cohu 1322-1000/EH13® and the target images were digitized as B/W at 8-bit resolution using a Videum AV Frame Grabber®. All settings of the frame grabber were left at default and a sampled digitized image is shown in Figure 5. If the CCD camera under this test is able to perfectly capture the pattern, the grayscale of each step should increase in a log step due to the linear step density in the target. Figure 6 depicts a graph of pixel values of a cross section of the top step patterns. Notice that the overall graph follows a log relationship that we anticipated, but oscillations and noise can be clearly observed from the curve instead of clean log steps. Higher oscillation near the step boundaries is caused by the reflectivity transition of the discrete step patterns that influence the CCD sensor resolution of detection where Gibbs phenomenon is present. These noise levels clearly indicate that CCD cameras have a limitation in measuring luminance. To test how accurately the average of each field follows the theoretical curve, the average of each step field was plotted using a log graph along with a linear fit line and shown in Figure 7. Notice that the average follows reasonably closely to the ideal log linear line. This suggests that using the average of pixel values is more reliable than using individual pixel values in computing luminance of targets for visibility measurements. The actual average and standard deviation of each step density is summarized in Table 1.

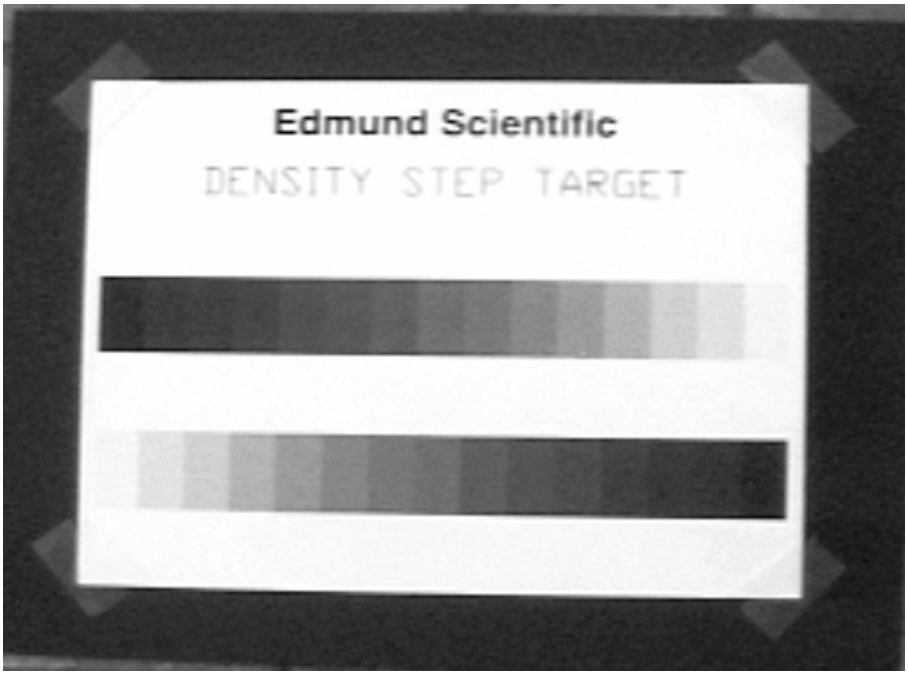

Figure 5: Image of EIA 20:1 Step Density Target taken by Cohu 1322-1000/EH13 Color Camera

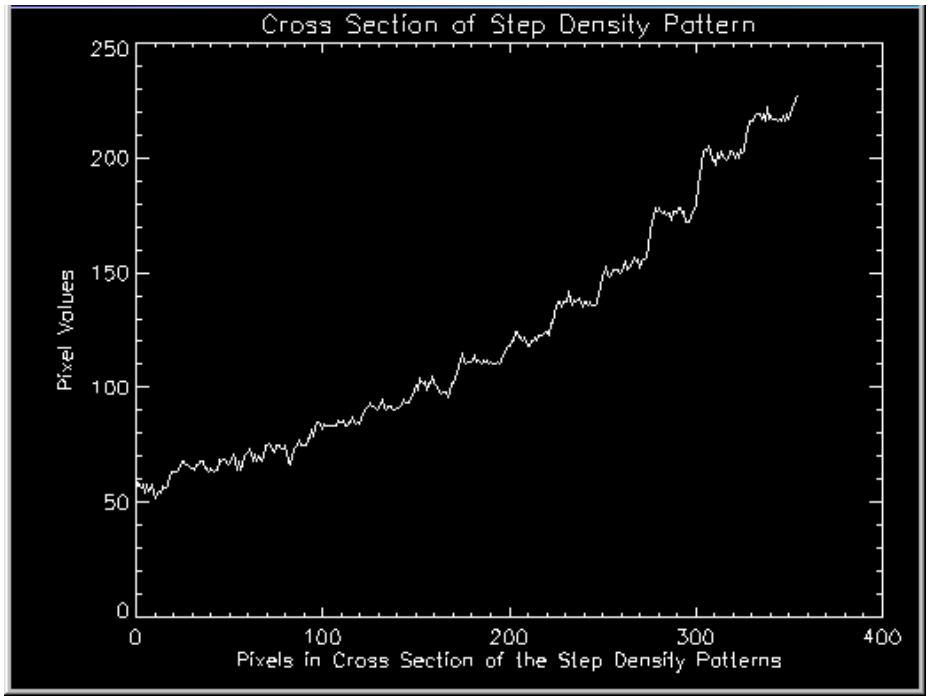

Figure 6: Pixel values of step density patterns

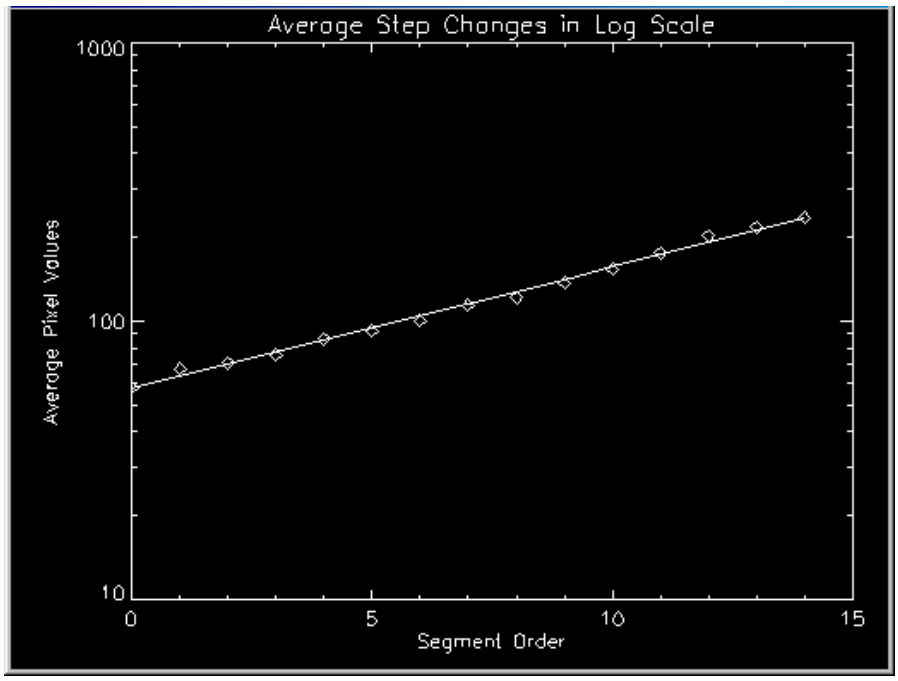

Figure 7: Log scale plot of average pixel values in each step density that fits to a linear line

Table 1: Average and standard deviation of pixel values in each field and linear fit error in transmission

Step Field	Avg Pixel Value of Step Field	Standard Deviation of Step Field	% Transmission	
			Average Luminance (%)	Linear Fit Error (%)
1	57.7685	4.28384	22.6543	0.180242
2	67.6265	3.50483	26.5202	1.67043
3	70.7076	3.23992	27.7285	0.251854
4	75.7280	2.97792	29.6973	0.683869
5	86.1740	2.60147	33.7937	0.201048
6	92.1736	2.56739	36.1465	0.997180
7	100.646	2.93708	39.4688	1.60128
8	114.293	3.16833	44.8210	0.590590
9	121.890	2.65945	47.8001	2.41186
10	137.322	2.96177	53.8517	1.66806
11	154.193	2.96306	60.4679	0.920817
12	176.318	2.78168	69.1443	1.26625
13	202.387	2.30709	79.3676	4.31431
14	218.193	2.06313	85.5659	2.57884
15	235.834	1.78900	92.4839	0.724427

3.2 Analysis of Visibility Measurement Limitation on Single and Multiple Targets Using Video Images

It was shown in Section 3.1 that resolution of luminance levels in CCD video cameras is limited by the noise levels. Dynamic range of pixel values is less than the ideal range of 0 to 255. This section presents a theoretical analysis on the visibility measurement limitations related to the number of targets under the assumption of ideal targets that lead to ideal measurement of contrasts. This theoretical analysis is supported by actual data.

The most fundamental visibility principle is Duntley's law [1] that is expressed as

$$\frac{C}{C_0} = e^{-\sigma d} \tag{1}$$

where C_0 is the inherent contrast, C is the contrast of an object or target of observing, σ is the extinction coefficient, and d is the distance from observer to the object. This relation can be adapted to digitized images obtained from cameras. First assume that the digitization is done at 8-bit which ranges from values of 0 to 255. With this range of gray scale, it is also safe to assume that the range is normalized to [0, 255]. For simplification, we further normalize this range to [0, 1]. This simplification gives the following relation:

$$C_I = e^{-\sigma d} \tag{2}$$

where C_I is a normalized contrast obtained from an image. Just noticeable contrast is defined as $C/ C_0 = 0.05$ which is translated to $0.05 * 255 = 12.75$ of luminance difference in pixel values that create contrast. This just noticeable contrast is the distance in which the visibility is determined. This value is used for a contrast threshold for computing visibility. Therefore, we arrive at a relation:

$$\sigma = 3/V \tag{3}$$

where V denotes visibility, i.e., distance, and σ is inverse of distance. Two cases are studied based on this normalized assumption.

Case 1: Unlimited number of targets at all distances
Under the normalized assumptions, we would like to explore the question, "How does the contrast of targets at different distances vary under different visibilities if an unlimited number of uniform identical targets are placed?" Assume that the targets have a simple shape as shown in Figure 8 where the normalized inherent contrast is 1, which is computed from digitized average pixel values between black and white areas.

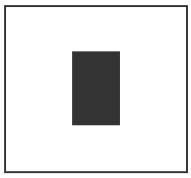

Figure 8: Ideal target with normalized inherent contrast, 1, between black and white

Assume that targets are arranged at all different distances. In order to see how the contrasts of these targets change under different visibility conditions, we first need to compute extinction coefficients for various visibilities using Eq. (3). We pick the following values: for V = 100m, $\sigma = 3/100 = .03$; for V = 200m, $\sigma=3/200=.015$; for V=300m, $\sigma=3/300=.01$; for V=400m, $\sigma=3/400=0.0075$; for V=500m, $\sigma=3/500=.006$. Using Eq. (2) and the computed extinction coefficients, normalized contrasts can be computed by substituting distances between 0 to 500 meters. The resulting graph is shown in Figure 9.

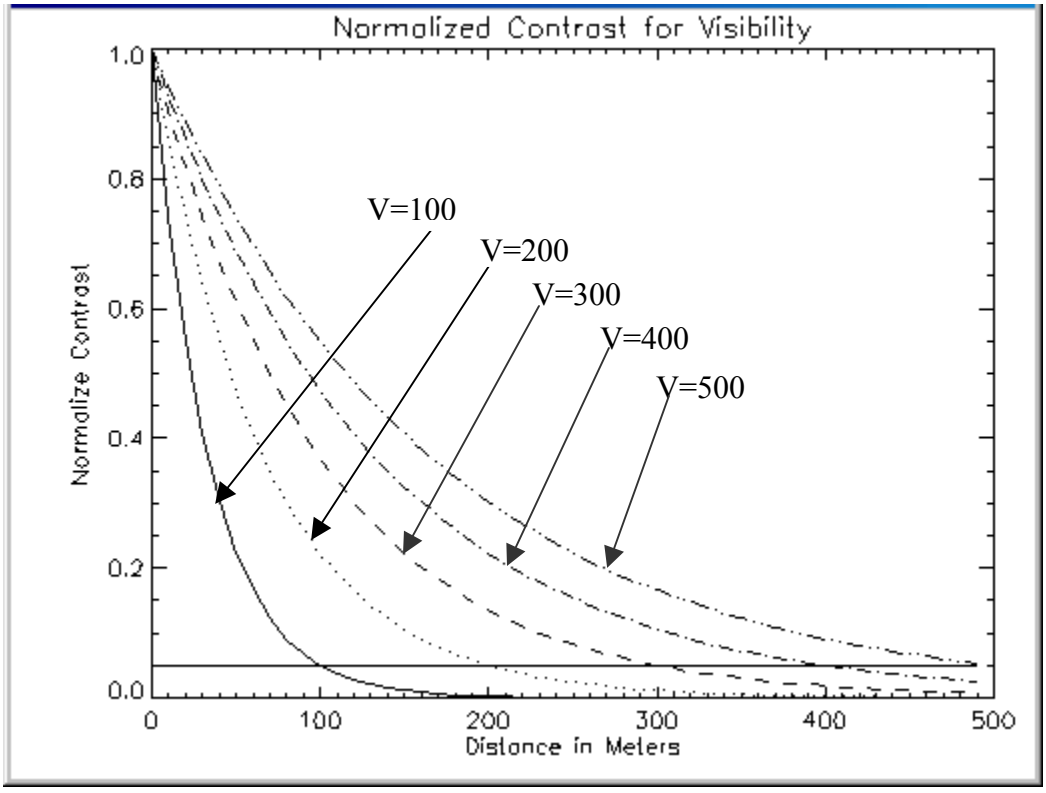

Figure 9: Contrast changes of targets at all distances under selected visibility conditions

The horizontal axis denotes the distances of targets. The horizontal line at normalized contrast 0.05 is a threshold level of contrast that determines visibility in terms of meters, i.e., any target's contrast that drops below 0.05 is considered not visible. Notice from Figure 9 that the contrast drops more quickly as visibility becomes lower. It is also obvious that targets located at a distance farther than visibility cannot contribute in measuring visibility. For example, if visibility is 100 meters, all targets located beyond 100 meters cannot be used for computing visibility. This would be the first limitation of the observation.

Case 2: Limited number of targets at selected distances

Suppose that targets are placed at distances 10m, 20m, 40m, 100m, 150m, 200m, and 300m. The question we wish to explore next is, "How does the contrast of each target change under various visibility conditions?" This means that the variable *d* in Eq. (2) must be fixed for each target, and the extinction coefficient σ should be varied for the selected target. Hence, the contrast for each target follows the relation:

$$C_I = e^{-(3/V)D} \tag{4}$$

where *D* is a constant that must be replaced for each target distance (distance from camera to target) and *V* is the visibility that must be varied for various visibilities. For each target, we varied the visibility from 0 to 1000 meters and the result was plotted in Figure 10. Again, the horizontal straight line at the normalized contrast 0.05 is the threshold that determines the visibility. Notice from Figure 10 that, if visibility is below the target distance, the target is no longer visible. For example, the target at D=300m has less than 0.05 contrast if visibility is lower than 300m and will not be visible. Notice also that contrasts tend to quickly saturate if visibility becomes much higher than the target distance. This means, for example, the target at 10m will not be able to provide measurable contrast differences if visibility is higher than 100m.

Using Figure 9 and 10 graphs, we can draw some important conclusions regarding the measurement limitation of visibility using a fixed number of targets. Suppose that we are allowed only one target to measure visibility from 10m to 500m. Then the target must be placed at 10m since any target placed beyond 10 meters will not be visible at visibility 10m. This can be verified from Figure 9 by placing a vertical line at 10m, which would cross all of the visibility lines. On the other hand, contrast changes of this target at 10m shown in Figure 10 suggest that accuracy will be very low under higher visibility conditions using this target. For example, this target's contrast will not change much when visibility changes from 400m to 500m.

The conclusion is that, in order to be able to measure visibility in a wide range, uniform targets must be placed at a wide range of distances. Using only a single target will severely limit the measurement accuracy and range, and more targets at varying distances will increase the measurement range and accuracy according to the inspection of graphs.

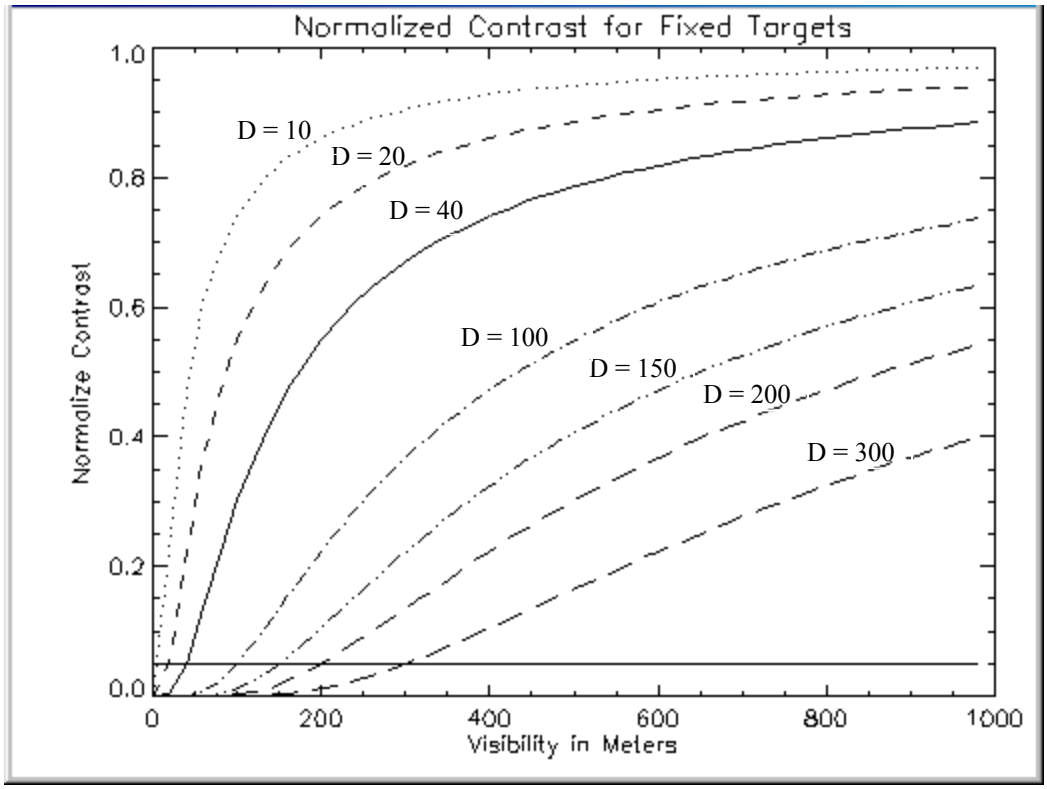

Figure 10: Contrast changes of targets under various visibility conditions

In order to verify whether the theoretical curves obtained in Figure 10 from Case 2 actually exist under real varying visibility conditions with real targets or not, real world data was analyzed. We picked a day that had visibility recoded from 60 to 490 meters. A target at 100m was selected. Its contrast data, computed by the differences of luminance between white and black area of the target, were plotted in Figure 11. Notice that the normalized theoretical contrast curve at D=100 in Figure 10 is roughly equivalent to the real world data shown in Figure 11. Although they are not shown, similarities were observed from the targets at other distances.

From this normalized contrast analysis, we can also learn that luminance values of camera images are equivalent to normalized values within the calibrated camera range. This suggests that equivalent normalized contrast can be obtained by the differences of luminance values between the white area and black area.

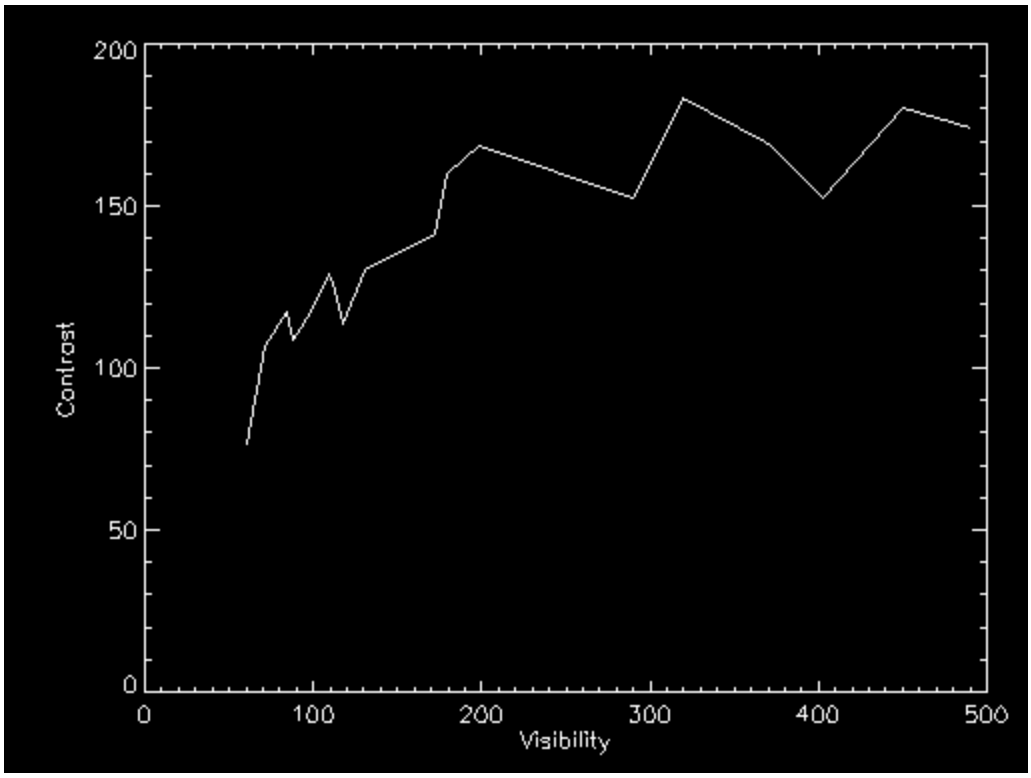

Figure 11: Contrast change of target at 100m for various visibility conditions

CHAPTER 4: NIGHT VISIBILITY EXPERIMENTS USING NEAR IFRARED SOURCE AND TARGETS

4.1 Introduction

This chapter describes the results of experiments performed using Near Infrared (NIR) light sources and cameras for night visibility study during this project. NIR cameras sense a wide range of spectrum typically ranging 400-1,000nanometer (nm) with low cost. Using NIR cameras, objects are recognizable under low lighting conditions (as low as 0.05 LUX) and the images are not distorted as much as the case in deep IR cameras. The question we wish to answer is, "Can NIR cameras be used for measurements of night visibility?" Three different types of apparatuses were tested for this study: (1) No NIR light source, (2) NIR light source attached to target, and (3) Target illumination using NIR light source. The target was set up at 10m from the camera that had a focal length of 3.6millimeter (mm). In a few experiments, we found that the NIR camera we used was not able to see the target without any light source on dark nights. Therefore, the second and third options (that utilize an active NIR light source) were rigorously tested, and the result is presented in this chapter.

4.2 NIR Illuminated Target

Since the NIR camera used was not able to see the target on dark nights, the first option was to illuminate the target using an NIR light source. The NIR source was set up on the pole where the camera was mounted. Two square box units shown in Figure 12 are the NIR light sources that were mounted on the pole. This NIR source produced 840nm NIR light within a range 10m. Figure 13 shows one of the images captured by the NIR camera. The target is shown in the right side of the image with a faint white stripe.

The hypothesis we wish to test in this experiment was that the contrast of the NIR illuminated target would be lower as visibility becomes lower. This hypothesis is based on the reasoning that, if visibility becomes lower, only a partial amount of NIR light will be able to reach the target since the NIR light rays will be scattered by air particles. Reduced light rays scattered on the target in turn reduce the contrast of the target.

Figure 12: NIR light source mounted on the camera pole

Figure 13: NIR source illuminated target

To test this hypothesis, images were organized into visibility range from 130m to 490m. Contrasts of the target area were computed and plotted, which is shown in Figure 14. Notice that the curve is noisy, but it can be clearly observed that the basic principle of contrast reduction relation of visibility demonstrated in Chapter 3 holds, i.e., its curve follows an exponential relation shown in Figure 10. This proves that the hypothesis is correct. In the graph, the noise was largely due to the headlights of vehicles passing by the highway because the target was set up along the highway. One approach of solving this noise problem would be using modulated light sources and adding a demodulation filter to the camera. Such experiments were not performed due to limited budget and time.

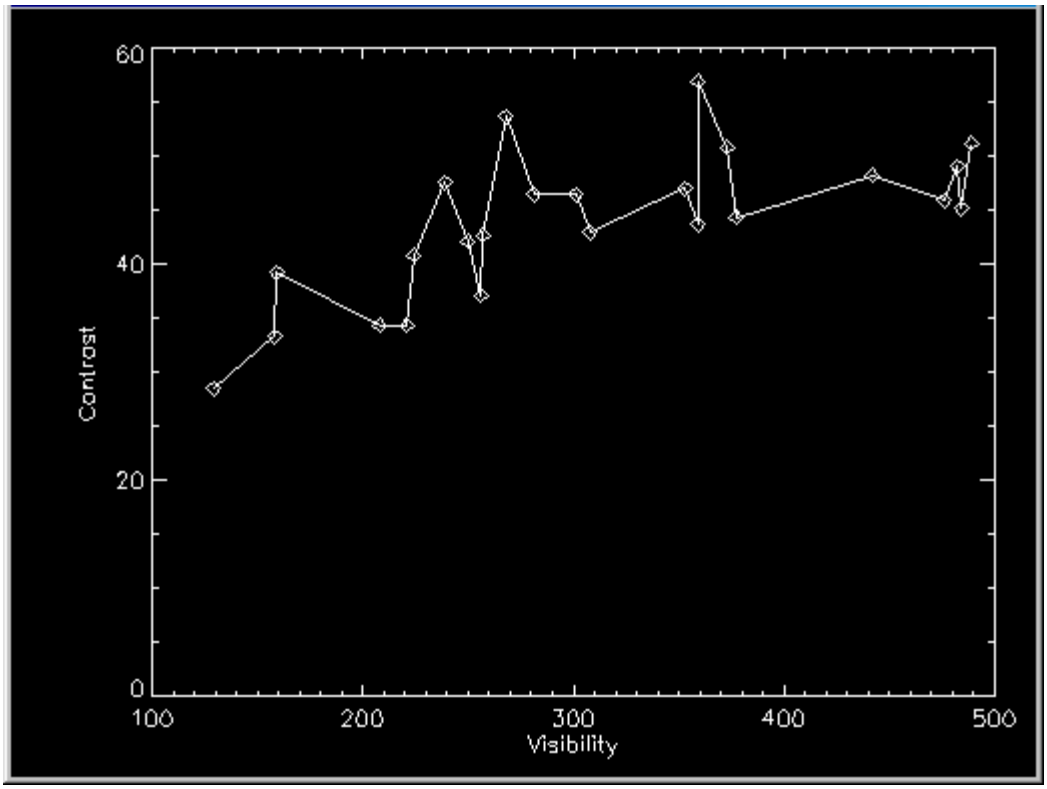

Figure 14: Visibility VS Contrast plot of NIR illuminated target

4.3 NIR Light Source Attached to Target

In this experiment, the NIR light source was directly attached to the target with a 45 degree angle from the target surface as shown in Figure 15. The hypothesis we wish to test in this experiment is that, as visibility decreases, the NIR light source attached on the target will be more scattered causing the NIR camera to capture more luminance. More specifically, the summation of luminance in the target should increase, as the visibility becomes lower.

Figure 15: NIR light source attached target

Figure 16 shows an example image of the NIR light source attached target seen by the NIR camera. The small white circle is the light source and the tail is the amount of light scattered by atmospheric conditions.

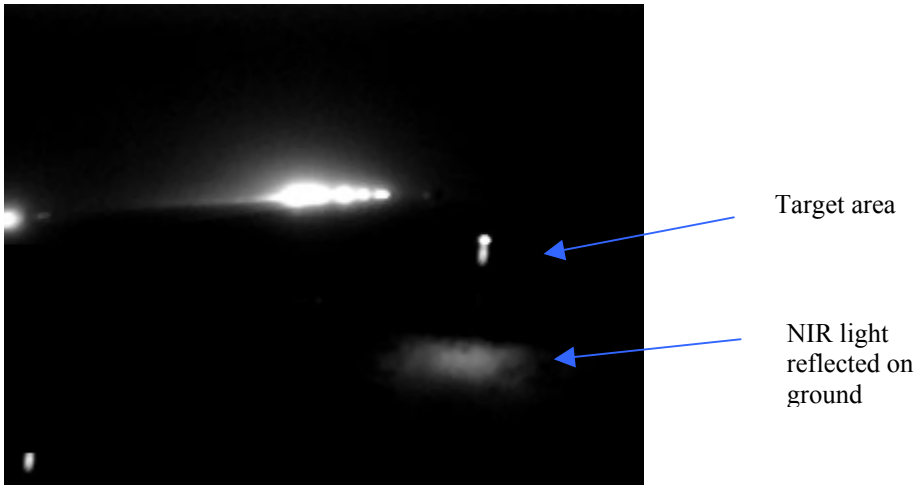

Figure 16: A sampled image of NIR source attached target

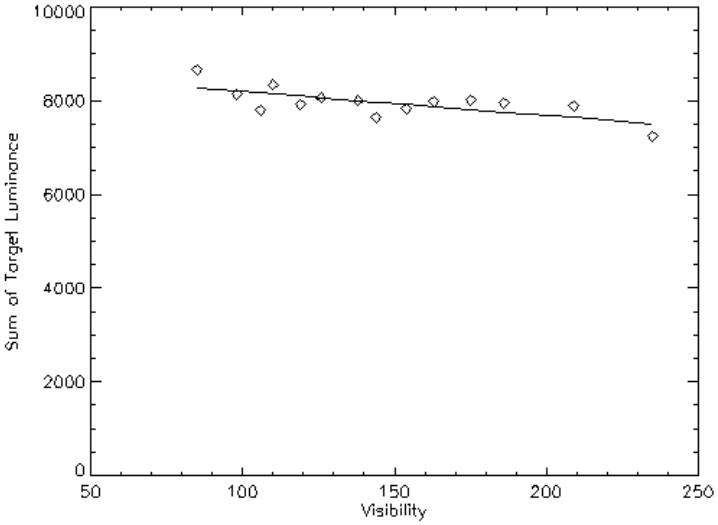

Figure 17: Visibility versus luminance sum of NIR attached target

A plot of visibility against sum of luminance in the target area is shown in Figure 17. In Figure 17, a clear trend can be noticed, i.e., target luminance decreases as visibility increases. Therefore, the hypothesis of this experiment is proven correct. However, noise effects by surrounding light sources can be also observed.

Using the same setup and images collected, the luminance reflected on the ground by the NIR light source was tested. The NIR reflected ground area was covered with grass. We found that the texture of grass blades have an interesting property that NIR lights are evenly reflected as shown in Figure 16. Moreover, the area becomes brighter when air has less opacity and becomes darker when air has more opacity since the amount of NIR lights can reach to the reflected area is limited by air opacity. Therefore, the sum of luminance in the reflected area is a function of transmissivity or visibility. Figure 18 shows the plot of visibility versus sum of luminance. Notice that there is a linear relation with some noise, but the trend is clearly tighter than the measurement of luminance from the NIR attached target. These observations suggest that measuring the luminance of NIR reflected targets could provide a good way of measuring night visibility. We also tested images obtained by pointing the NIR light source directly to the NIR camera, but pixels in the images were completely saturated and therefore not desirable.

Among the various methods tested using NIR light sources and camera, the measurement of air opacity using the intensity of NIR reflected on a special pattern (grass blades) gave the most reliable correlation with visibility. This approach can be improved by two additional changes in the apparatus. First, it is recommended that an NIR band-pass filter be mounted on the NIR camera since it will cut off the noise in the range of visible spectrum produced by headlights of passing vehicles. Second, a more uniform reflector pattern that has a similar texture as grass blades should be placed. It is expected that these two changes will drastically improve the accuracy of night visibility measurements.

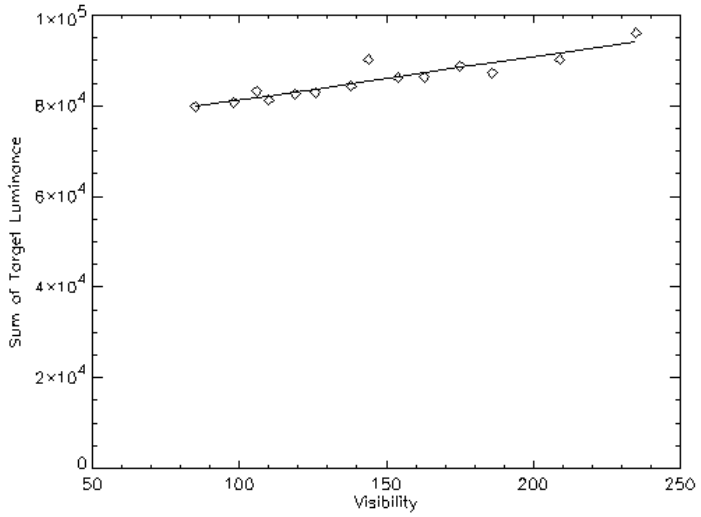

Figure 18: Visibility versus the sum of reflected light source

CHAPTER 5: RELATIVE VISIBILITY AND COMPUTATIONAL METHODS

5.1 Introduction to Relative Visibility

Sections 1.2 and 1.3 discussed why absolute measurements cannot effectively express true atmospheric visibility and why relative visibility (RV) can provide a better representation. We briefly revisit the issue in this section and formally establish the definition of RV.

Atmospheric visibility is an essential part of information to gauge navigational difficulties and risks that are associated with reduced human visible information caused by poor atmospheric conditions. Visibility measurements are, therefore, important and should be a good measure of difficulties or disruption of visible information caused by atmospheric conditions. However, nearly all visibility meters today rely on measurements of one or two of many atmospheric parameters, and the measurements often do not match what the human eye sees. This is because they are measuring just one or two of the many causes that affect the visibility rather than directly measuring the amount of visible information. For an illustration, consider a visibility meter design based on light-scatter measurements, since most commercial visibility meters are designed that way. If we measure visibility using such instruments, one on a dark night and another in a bright daylight, they would report an identical visibility as long as the density and sizes of atmospheric particles that affect light scatter are the same. For the human eye, visibility is clearly reduced at night because the distance you can see is much shorter. Snowy and rainy conditions also cause similar types of errors [12]. Such discrepancies between what the human eye sees and what the visibility meters report have been a major problem for developing critical safety applications based on visibility. Visibility measurements are simply not trustworthy.

The fundamental problems with the present approaches are twofold. First, we understand that visibility is affected by many atmospheric and environmental factors. However, any attempt to measure every possible cause that affects visibility would be neither practical nor economical. Second, spatial variants in visibility present additional problems, i.e., visibilities can quickly change from one location to another, and any single measurement of atmospheric parameter can only represent a single spot of the area. On the other hand, the human eye uses the whole region of interest to sense the visibility. Therefore, there are two challenges in increasing accuracy of visibility measurements in a conventional way: (1) find every possible cause that affects visibility and develop the measurement instruments, and (2) find an economical way of measuring spatially variant visibility. Both challenges are impractical and nearly impossible to meet.

The fundamental problem with the conventional ways of measuring visibility lies in trying to *indirectly* measure visibility using atmospheric conditions. Moreover, conventional definitions of visibility itself present an additional problem in that the spatially variant nature of visibility cannot be effectively expressed by a single parameter.

To resolve the visibility issues discussed, we introduce a new parameter referred to as the **Relative Visibility** (**RV**) that represents a relative amount of visual information observable in reference to the amount of visual information at the same location on an ideal clear day. For simplicity, RV is represented by percent or equivalently using a real number between zero and one. Zero percent of RV means that no visual information is available, e.g., total whiteout or blackout conditions. RV increases as the objects in the area are more clearly visible to human eye, or as the visual condition improves. One hundred percent of RV means that the present condition is identical to the ideal clear condition. Hence, RV represents how close the measuring visual condition is to the ideal condition. It should be noted that RV reference depends on the viewing area or region of interest that is determined based on applications. To clarify the region of interest, we further define RV into Motorists Relative Visibility (MRV) for ground transportation applications. For motorists, important visual information is not clouds in the sky but road boundaries and vehicles ahead. Hence, MRV should be measured using visual information needed for vehicle driving, and the measure of MRV should imply road boundaries and surroundings as the region of interest (ROI). For an actual usage example, 50% MRV should mean that motorists' effective visual information for driving has been reduced to 50% in comparison to that of an ideal condition. For other applications such as aviation, we may introduce the term Aviation Relative Visibility (ARV) to limit the scope to towers and runways. The scope of this report is limited to ground transportation, thus the discussions in this report are limited to MRV.

5.2 Motorists Relative Visibility (MRV)

MRV should describe how clearly the road geometry and surroundings are visible to the motorists in reference to an ideal clear day. Presently, video cameras or digital cameras that work in visible spectrum are the only type of sensors that can capture visual information. Therefore, MRV measurement methods in this project were studied using video images with an assumption that the visual information captured through a forward-looking video camera is an estimate of what a typical motorist sees through the front windshield of a vehicle. This is a gross simplification, since human vision is based on a stereoscopic system where 3-D information is available. Moreover, human perception of visibility is based on object recognition with distance estimates based on 3-D information, which is not available from 2-D video images. On the other hand, video images provide a reasonable estimate since MRV measurements are only intended for obtaining relative measurements that estimate visual characteristics that contribute to a reduction of human visual information. However, MRV measured from video images would not represent one to one mapping or quantification of human perception until video technologies and signal processing techniques advance to creating a system equivalent to human vision.

First, we introduce an index referred to as the **Motorist's Visual Index (MVI)** that represents measurable visual characteristics and clarity from video images. The details on how to compute MVI are presented in Section 5.3. Let MVI measured at a location l at time t be denoted as $MVI(l,t)$. Suppose that MVI was computed using an

image taken under an ideal visual condition, i.e., a clear day with no cloud cover and no obstruction of view. Let this MVI be denoted as $MVI_{opt}(l)$, then it should satisfy:

$$MVI_{opt}(l) = \underset{t}{Max}\, MVI(l,t) \tag{5}$$

Using measured MVI, MRV is then formally defined as

$$MRV(l,t) = 1 - \frac{MVI_{opt}(l) - MVI(l,t)}{MVI_{opt}(l)} \tag{6}$$

Notice that the range of MRV is [0,1]; the maximum occurs when $MVI_{opt}(l) = MVI(l,t)$; the minimum occurs when $MVI(l,t)=0$. Essentially, MRV represents a parameter in which how close the measuring video image is to the image taken under an ideal condition in terms of the image features extracted by MVI. This also indicates that, as long as we can compute MVI from images or other means, MRV can be easily obtained using Eq. (6). In the following section, MVI computational methods are presented.

5.3 MVI Computation from Video Images

5.3.1. Theoretical Derivation of MVI

Ideally, MVI should be a linear function of atmospheric visibility. However, in order to be able to measure atmospheric visibility from video images, the distances of the objects or pixels in the image must be known. Unfortunately, such distance information is lost during the 2-D video imaging process and cannot be recovered from the image alone, unless specific distances and inherent contrasts of the object are known. Therefore, an alternative approach sought in this project is computing the factors that influence visibility, such as reduction of edge information and contrast trends in the area that has a property of 2-D images projected with measurable distance changes.

In order to extract features that affect atmospheric visibility from images, we start the derivation from the fundamental principle of visibility in atmosphere. One of the most fundamental principles governing visibility under uniform distribution of air particles is expressed using luminance of a black target against horizon sky as [2,3]:

$$L_b = L_b^0 e^{-\sigma x} + L_h(1 - e^{-\sigma x}) \tag{7}$$

where L_b^0 is the inherent luminance of a black target that is non-zero; L_b is the apparent luminance of the target; L_h is the luminance of horizon sky; σ is the extinction coefficient (inverse of distance function); and x denotes the distance from the target to the observation point. The first term describes exponential decay of inherent luminance of

the target as a function of distance and atmospheric conditions, and the second term describes the air light changes.

Assume that an object A has background B. Writing the luminance relation, Eq. (7), for A and B and finding the difference of luminance gives:

$$L_A - L_B = (L_A^0 - L_B^0)e^{-\sigma x} \tag{8}$$

where L_A and L_B are the apparent luminance of A and B, and L_A^0 and L_B^0 are the inherent luminance of A and B, respectively. Using a difference notation, Eq. (8) can be simply written as:

$$D_{AB} = D_{AB}^0 e^{-\sigma x} \quad . \tag{9}$$

The difference D_{AB} essentially represents a contrast formed by foreground A and background B in an image. If visibility *V,* i.e., the distance from camera, is determined at a threshold $\varepsilon = D_{AB} / D_{AB}^0$, which would be the point where the difference between the foreground and background is no longer distinguishable, then the visibility is computed from Eq. (9) by replacing x with V, i.e.,

$$V = -\frac{\ln \varepsilon}{\sigma} \quad . \tag{10}$$

This principle given in Eq. (10) has been the basis for nearly all visibility studies and instrumentations that have been developed [2]. It should be noted that ε is always less than 1 since $D_{AB} \le D_{AB}^0$, resulting a positive visibility. This relation obtained for the standard definition of contrast is referred to as the Koschmieder's rule [2,3], that is, if contrast is defined as:

$$C_{AB} = \frac{L_A - L_B}{L_B} \quad . \tag{11}$$

Coming back to our focus, Eq. (11) normalization is not necessary in video images, since pixel values are already normalized within the sensing range when the image of real-world scene is converted into a digital form.

For simplicity, let C_x denote the apparent contrast of an object and C_x^0 the inherent contrast of the object at distance x. Then Eq. (9) under a uniform extinction coefficient can be rewritten as:

$$C_x = C_x^0 e^{-\sigma x} \tag{12}$$

This relation was first derived by Duntley [5], which enabled visual-range measurement from any background using the contrast reduction instead of horizon sky.

Next, consider a line of sight from the camera that linearly increases the distance, and integrate the contrasts along the selected line from zero to infinity, i.e.,

$$\int_0^\infty C_x dx = \int_0^\infty C_x^0 e^{-\sigma x} dx = \frac{C_x^0}{\sigma} \tag{13}$$

It is assumed that the inherent luminance C_x^0 is a constant, which would be equivalent to placing objects with the same contrast along the line that linearly increases the distances from the observation point. Since the inverse of extinction coefficient is proportional to visibility as shown from Eq. (10), the following relation holds:

$$\int_0^\infty C_x dx \propto V \tag{14}$$

Eqs. (13) and (14) tell us that atmospheric visibility is strongly correlated (linear) to integration of contrasts, if objects with the same contrast can be placed in a straight line. However, such a set up would be expensive. Early research by Kwon [11] showed that few targets with an identical contrast can be used for the estimation of atmospheric visibility using Eq. (14).

In order to further examine the visual-range principles, consider that images are taken at the same location under different visual range conditions. Let two extinction coefficients be σ_1 and σ_2, and the corresponding observed contrasts be $C_{x,1}$ and $C_{x,2}$, respectively; then the following relations holds,

$$\frac{1}{\sigma_1} = x \ln \frac{C_{x,1}}{C_x^0} = V_1 \tag{15}$$

and

$$\frac{1}{\sigma_2} = x \ln \frac{C_{x,2}}{C_x^0} = V_2 \tag{16}$$

where V_1 and V_2 denote two different visibility conditions and C_x^0 is the inherent contrast at distance x. Suppose that two conditions are compared by simple subtraction, that is,

$$V_1 - V_2 = x(\ln C_{x,2} - \ln C_{x,1}) \tag{17}$$

Note from Eq. (17) that, when two images taken at the same location are compared, inherent contrasts are no longer a factor, but distance information is needed. More specifically, when two identical locations are compared, distance and the contrasts are the only parameters that we need to know for comparison of two different visibility conditions. Therefore, simple measurements given in the following form computed over a region of interest can be used as MVI for computing MRV.

$$V \approx x \ln C_x \tag{18}$$

From Eq. (18) we can draw important information that the contrasts and distances of the objects in an image are the key factors that directly influence visibility and must be included in the computation of MVI. We extend this analysis by introducing a threshold of contrast. Based on the definition of visibility shown in Eq. (10), visibility is determined at a threshold, $\theta = C_x / C_x^0$, where the object and background are no longer distinguishable, which means visibility can be directly computed by

$$V = x \ln \theta, \tag{19}$$

if we can find an object at the threshold and the distance. In fact, if we let $\ln \theta = 1$, then x would be the visibility, which follows the basic definition of visibility in Eq. (10). To extract this threshold information from an image, we define an indicator function I_x as

$$I_x = \begin{cases} 1 & \text{if } \mathrm{C_x} \geq C_\theta \\ 0 & \text{if } \mathrm{C_x} < C_\theta \end{cases} \tag{20}$$

where C_θ is a threshold in which inherent contrasts of all objects in the image are greater than this value. Suppose that we choose a line that linearly increases in distance and compute the indicator function I_x, then it is clear that

$$V \propto I_f = \sum_x x I_x \,. \tag{21}$$

Since I_x is directly computable from the images using Eq. (20), Eq. (21) is computable if we can estimate the distances in the image. If we assume that roads are flat, the distance of pixels in the image may be estimated using the camera angle to a flat road model and the focal length of the camera. This estimation technique is described in Section 5.3.3. In Eq. (21), I_f essentially quantifies the amount of recognizable objects in the image since we can recognize objects when the contrast is above the recognizable threshold.

There are other factors that influence visibility in an image. Because visual range is reduced more by light scatter than absorption when visual range is reduced, the average luminance approaches the luminance of horizon sky. More specifically, within a certain luminance range the following relation holds,

$$V \propto L_{\max} - L_{av} \tag{22}$$

where $L_{\max}$ is the maximum luminance that corresponds to the horizon sky and L_{av} is the average luminance of the image. As long as the images are taken at the same location

with the same objects, Eq. (22), i.e., overall luminance is another factor that influences visibility.

Yet, another factor that also influences human visual information is the acuity of the objects in the scene. Such information can be estimated through the amount of edge information [16,17]. Therefore, the acuity factor can be estimated through the average contrast or variance of luminance.

By combining the three factors discussed, we construct a formula for computing MVI using the following relation:

$$MVI = f_1(I_f) + f_2(L_{av}) + f_3(C_{av}) \tag{23}$$

where f_i are control functions for each component, I_f quantifies the amount of recognizable objects, L_{av} is the average luminance measured in the image, and C_{av} is the average contrast of the image. The contrast average, C_{av}, may be replaced with a variance of the image depending on whichever computation is efficient. The choice of control functions of each component is discussed in Section 5.4.

5.3.2. Contrast Computation from RGB (Red Green Blue) Color Images

Images collected from most video cameras are produced in an RGB color space. RGB color space is represented by red, green, and blue primaries as orthogonal axes. Although contrasts may be computed using luminance conversion from the RGB color space, it loses the information on color contrast that the human eye perceives. For example, yellow lines in a pavement do not show as significant contrast as the human perceives when the color is converted to gray scale. Therefore, a more desirable approach would be directly computing the color contrast from the RGB space. Unfortunately, RGB color primaries were developed for color reproduction of monitors, and some portions of colors do not scale like human color perception [13].

For standardization of color sets, the CIE (Commission Internationale d'Eclairage) set up three hypothetical primaries, XYZ, which is referred to as CIEXYZ. The resulting color representation is that all visible colors are in the positive octant in the integration of matching functions being equal, and in the Y function matching the luminance efficiency function. Although the color specification in the CIEXYZ color space is useful for color reproduction, it is not useful for evaluating relative color changes or human perception of color contrast [13]. Therefore, other alternative color schemes have been developed such as L*u*v* and L*a*b* [13, 14]. One practical approach was proposed by Mayer (1988) [15]. He examined the sensitivity of the visual system and derived a set of color axes that pass through the regions where the tristimulus are most likely to occur [13, 15]. He calls this coordinate system the AC_1C_2 space. The AC_1C_2 color space was adapted for our color contrast computation in this project.

For actual computation of the AC_1C_2 color space, RGB is first converted to CIEXYZ using the following translation,

$$\begin{bmatrix} X \\ Y \\ Z \end{bmatrix} = \begin{bmatrix} 0.412453 & 0.357580 & 0.180423 \\ 0.212671 & 0.715160 & 0.072169 \\ 0.019334 & 0.119193 & 0.950227 \end{bmatrix} \begin{bmatrix} R \\ G \\ B \end{bmatrix} \tag{24}$$

Next, the AC_1C_2 color space is derived using the following mapping:

$$\begin{bmatrix} A \\ C_1 \\ C_2 \end{bmatrix} = \begin{bmatrix} -0.0177 & 1.0090 & 0.0073 \\ -1.5370 & 1.0821 & 0.3209 \\ 0.1946 & -0.2045 & 0.5264 \end{bmatrix} \begin{bmatrix} X \\ Y \\ Z \end{bmatrix} \tag{25}$$

With the color conversion to the AC_1C_2 color space, color contrasts of objects can be computed using the geometrical distance in the color space because the color space is now converted into a space where human perception of color contrast can be uniformly evaluated. Let 3x3 segments or pixels of an image be denoted as:

$$\begin{matrix} P_1 & P_2 & P_3 \\ P_4 & P_5 & P_6 \\ P_7 & P_8 & P_9 \end{matrix}$$

where P_i denotes a vector of the three color components at segment location i. Then, one simple way of computing the point contrast in all directions at the center location 5 is:

$$C_5 = \frac{1}{4}|(P_1 + 2P_2 + P_3) - (P_7 + 2P_8 + P_9)| + \frac{1}{4}|(P_1 + 2P_4 + P_7) - (P_3 + 2P_2 + P_9)| \tag{26}$$

Another alternative is,

$$C_5 = \frac{1}{4}(|P_1 - P_2| + |P_2 - P_8| + |P_3 - P_7| + |P_4 - P_6|) \tag{27}$$

Yet, another alternative is,

$$C_5 = \frac{1}{2}|P_1 - P_9| + \frac{1}{2}|P_3 - P_7| \tag{28}$$

It should be noted that P_i can be a pixel value at the finest scale, but is not recommended for MVI computation. Rather the P_i should be computed from a small segment due to the noise effects discussed in Chapter 3 and object emphasis in visibility.

For example, we may select four pixels as the basic unit of segment and represent it using the average.

One implication of the contrasts defined in Eq. 26-28 is that the values computed are equivalent to a measure of edges in the image [16,17]. Thus, the color contrast computed as above integrates acuity of images, which is one of the desirable characteristics determining RV.

5.3.3. A Flat Road Model for Distance Estimation

As discussed in Section 5.3.1, distance information to each pixel or region is needed for MVI computation (e.g., Eq. (21)). In general, accurate distance computation from a 2-D image is extremely difficult even if it is possible, due to loss of information by 2-D projection of a 3-D real world in the imaging process. However, a rough estimate of distances may be computed if the road is assumed to be flat in the computing region and the camera characteristics and the pointing angle are known. This section shows how the distance can be estimated from an image using a 3-D to 2-D projection relation.

For convenience of description, we first define the symbols used as follows:

L_h : Camera lens height from the ground

CCD Size:

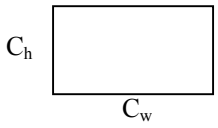

f: Camera focal length

$\phi_v^{\max}$: Camera vertical angle of view

$\phi_h^{\max}$: Camera horizontal angle of view

(P_x, P_y) : Pixel x and y position, the lower left corner is (0,0)

$(P_x^{\max}, P_y^{\max})$: Bound of pixel (x,y) position, the upper right corner.

T_d : Horizontal distance to target

ϕ_v^T : The angle from the vertical line to the target

ϕ_v^{Lower} : Lower bound of the vertical angle of view expressed in relation to the vertical line

ϕ_v^{Upper} : Upper bound of the vertical angle of view expressed in relation to the vertical line

T_{cd} : Parallel line distance from the camera lens to the centerline point that meets with the perpendicular line drawn from an object

T_{dd} : Direct line distance from the camera lens to an object

T_{pd} : Perpendicular line distance from the centerline to an object

ϕ_h^T : Horizontal angle from the centerline to an object

Consider that a camera with a CCD size of ($C_h \times C_w$) is mounted at a fixed height L_h and inclined towards the road with the degree of θ . It is assumed that the camera does not have left or right tilt, such that the lower side of CCD is parallel to the ground level. A target is assumed located at the horizontal distance T_d from the vertical line. This setup is illustrated in Figure 19.

Horizontal and vertical angles of view of the camera follow a simple trigonometric relation:

$$\phi_v^{\max} = \tan^{-1}(C_h / f) \tag{29}$$

$$\phi_h^{\max} = \tan^{-1}(C_w / f) \tag{30}$$

The lower and upper bounds of the vertical angle of view expressed in relation to the vertical line are then expressed as:

$$\phi_v^{Lower} = (90° - \theta) - \phi_v^{\max} / 2 \tag{31}$$

$$\phi_v^{Upper} = (90° - \theta) + \phi_v^{\max} / 2 \tag{32}$$

The vertical pixel position of the target is then computed by,

$$P_y = \frac{\phi_v^T - \phi_v^{Lower}}{\phi_v^{max}} P_y^{\max} \tag{33}$$

This relation provides an estimate of y-axis position on the CCD for the target position projected on to the CCD.

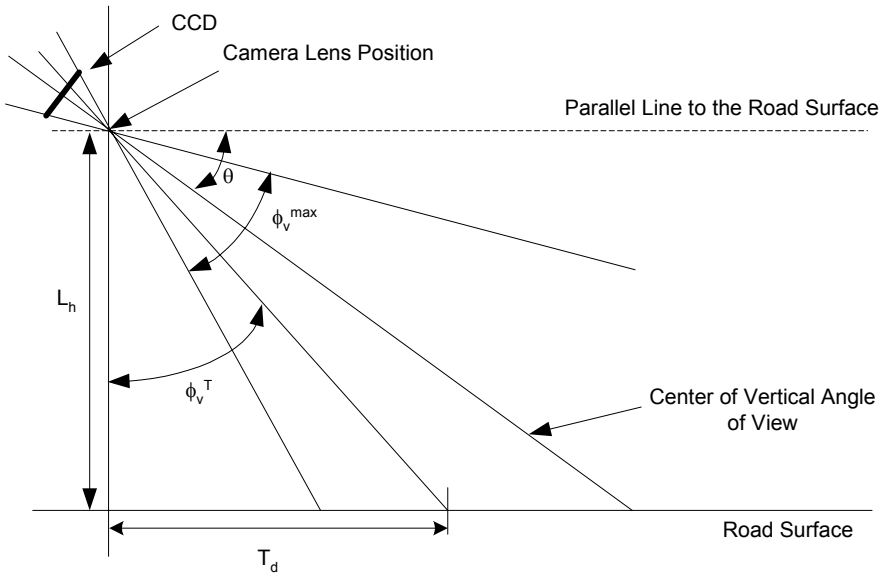

Figure 19: Side view of geometrical relation

Next, in order to find the mapping point to the x-axis of the CCD the top view of the geometrical relation is considered, as illustrated in Figure 20. The imaging area spans along with the left and right bounds of the horizontal angle of view of the camera. To create reference points, the imaging area is split in half using the horizontal centerline. A negative sign is assigned to the left side of the angles and distances from the centerline. A positive sign is assigned to the right side of the angles and distances from the centerline. Thus, the centerline is used as the starting point for both sides and has zero degrees and zero perpendicular distances along the line (see Figure 13 for a visual aid).

The parallel line distance from the camera lens to the centerline that meets with the perpendicular line drawn from an object, T_{cd}, has the following relation:

$$T_{cd} = \sqrt{L_h^2 + T_d^2} \tag{34}$$

Direct line distance from the camera lens to an object, T_{dd}, and the horizontal angle from the centerline to an object, ϕ_h^T, are then computed as:

$$T_{dd} = \sqrt{T_{cd}^2 + T_{pd}^2} \tag{35}$$

$$\phi_h^T = \tan^{-1} \frac{T_{pd}}{T_{cd}} \tag{36}$$

Similar to the vertical case, the horizontal pixel position of the target is obtained using the horizontal angle found, i.e.,

$$P_x = \left(\frac{\phi_h^T}{\phi_h^{\max}} + \frac{1}{2} \right) P_x^{\max} \tag{37}$$

where all parameters are now obtainable.

Next, we wish to estimate the distance from the camera lens to an object using a pixel position (x, y).

Since $\tan \phi_h^T = {T_{dd} \sin \phi_h^T} \big/ {T_{cd}}$, the final distance from the camera lens to the target is obtained as,

$$\begin{aligned} T_{dd} &= \frac{T_{cd} \tan \phi_h^T}{\sin \phi_h^T} \\ &= \frac{\sqrt{L_h^2 + (L_h \tan \phi_v^T)^2} \tan \phi_h^T}{\sin \phi_h^T} \end{aligned} \tag{38}$$

where

$$\phi_h^T = \frac{P_x - {1}/{2} P_x^{\max}}{P_x^{\max}} \phi_h^{\max}$$

and

$$\phi_v^T = 90° - \theta + \phi_v^{\max} \left(\frac{P_y}{P_y^{\max}} - \frac{1}{2} \right)$$

Notice that the final derivation in Eq. (38) is a function of all known values, i.e., pixel (x,y) position, horizontal and vertical angle of camera, and the camera angle in relation to the horizontal line. Therefore, an estimate of the distance from the camera lens to a target can be computed based on the pixel positions in the CCD. However, it should be cautioned that these estimates are based on a perfectly flat road model with no occlusion, which rarely occurs in the real world. Thus, one should accept a certain level of error in the final computed distances. Another point that must be mentioned is that human perception on distance is in a *log scale* like many other human perceptions. Thus, the distance computed by Eq. (38) should be implemented as a log scale.

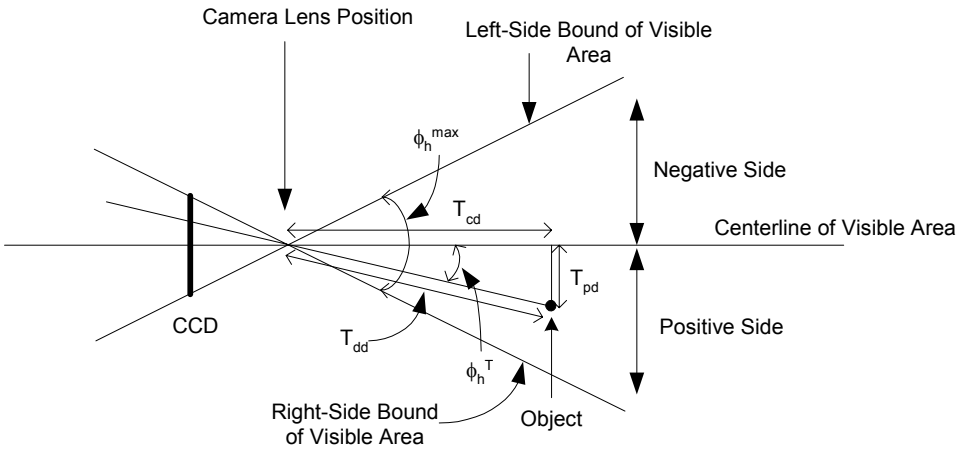

Figure 20: Top view of geometrical relation

5.3.4. Selection of Region of Interest For MRV Computation

A typical highway scene projected onto a CCD by a forward-looking camera may be divided into three regions as shown in Figure 21 (assumed one direction of a two-lane highway). Regions 1 and 3 represent the left and right shoulder of the road, respectively; and Region 2 represents the driving lanes. In Region 2, the number of vehicles on the lanes can significantly affect MVI instead of visual range or weather conditions. As a result, vehicles can create an effect of noise. Regions 1 and 3 are more stable in terms of object variability over time, such that visual information is most likely influenced by the atmospheric visual conditions. In particular, Region 3 has a better property in terms of distance information, because it shows better near distances than Region 1. Therefore, Region 3 is considered most desirable for MRV computation.

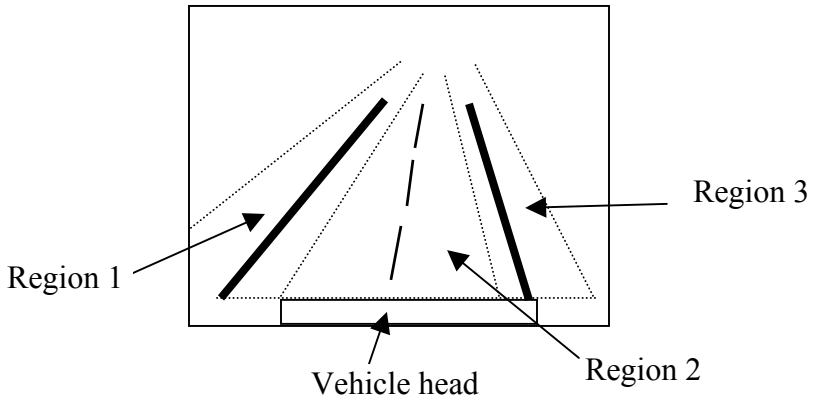

Figure 21: Region of interests in highway

5.3.5 Control Functions of MVI Components

In the MVI derivation in Section 5.3.1, Eq (23) essentially tells that MVI is a function of the amount of visible objects, the average luminance, and the average contrast in the ROI in an image, but the control functions were omitted in that derivation. In the following we show how to determine a sensible choice of a control function that closely models human perception from stimuli. Since MVI should be a measure of information on visible features, a sensible choice of control functions would be adapting a shape of an Entropy function, i.e., $f(x) = -x \log x$. This type of function has been used for quantifying information [18] and has an inverted cup-shape. Human perception typically has an optimal sensing level and exceeding or less than that optimal level reduces information, which follows an inverted cup shape curve.

Consider luminance in ROI. Visibility increases as the average luminance of ROI decreases up to a certain threshold that would be the optimal luminance point. If the average luminance drops beyond this threshold (which would be the same as objects under too dark light), visibility is rapidly decreased. A similar effect occurs for the average contrast. Visibility increases only up to a certain threshold level of contrast. If the average contrast reaches beyond this threshold, visibility begins to decrease again. In all cases, visibility is more rapidly decreased after passing the optimal threshold. This threshold effect can be estimated through a range controlled parabolic function with different rates of decreases from the optimal point. Without further discussion, we directly provide example control functions that were obtained from a color video camera we used in our experiments.

Control function for indicator function:

$$f_1(I_f) = \begin{cases} -(I_f - 10,000)^2 / 333,333 + 300, & \text{if } I_f \le 10,000 \\ -(I_f - 10,000)^2 / 1,000,000 + 300, & \text{if } I_f > 10,000 \end{cases} \tag{39}$$

Control function for average luminance:

$$f_2(L_{av}) = \begin{cases} -(L_{av} - 160)^2 / 85 + 300, & \text{if } L_{av} \le 160 \\ -(L_{av} - 160)^2 / 176 + 300, & \text{if } L_{av} > 160 \end{cases} \tag{40}$$

Control function for average contrast

$$f_3(C_{av}) = \begin{cases} -(C_{av} - 42)^2 / 20 + 300, & \text{if } C_{av} \le 42 \\ -(C_{av} - 42)^2 / 6 + 300, & \text{if } C_{av} > 42 \end{cases} \tag{41}$$

In the above control functions, the optimal points for I_f, L_{av}, and C_{av} are 10,000, 160, and 42, respectively. These optimal points could be derived from the images taken under an ideal lighting condition, i.e., a clear day with no cloud cover. The choices of actual values would be influenced by image resolution and camera characteristics.

5.4 Examples

This section provides a few examples of MVI computation. The first example shown involves computation of MRV from images produced by a fixed video camera from another visibility project [12]. The site was located at Interstate Highway I-35, Thompson Hill, Duluth, Minnesota. In the testing area, nine targets were present at distances of 5, 10.5, 20.1, 32.7, 67, 80, 100, 150, and 200 meters from the camera, which are numbered 1 through 9. The targets are only used as manual verification of visibility. For MRVI computation, Region-3 (right side of the road) in Figure 22 has the clearest view of the areas with time invariant objects capturing targets ranging from close to the camera to very far distances. Thus, Region-3 was chosen for MRV computation. Figure 23 depicts the computed MRV for the images taken on June 24, 1994 when low visibility conditions occurred. The ordinate numbering corresponds to the time specified in the caption. It can be observed that MRV was started from a low value of less than 0.2 at 4:59AM and then gradually increased. To show how MRV relates to the visible information, four sample images corresponding to ordinate numbers 1, 12, 17, and 20, are chosen shown in Figure 24 along with the computed MRV. The images are arranged as increasing MRV order. It can be clearly seen that, as MRV increases, the targets in the images are more and more clearly identifiable, which corresponds to higher and higher levels of visual information available to motorists.

Figure 22: ROI selection

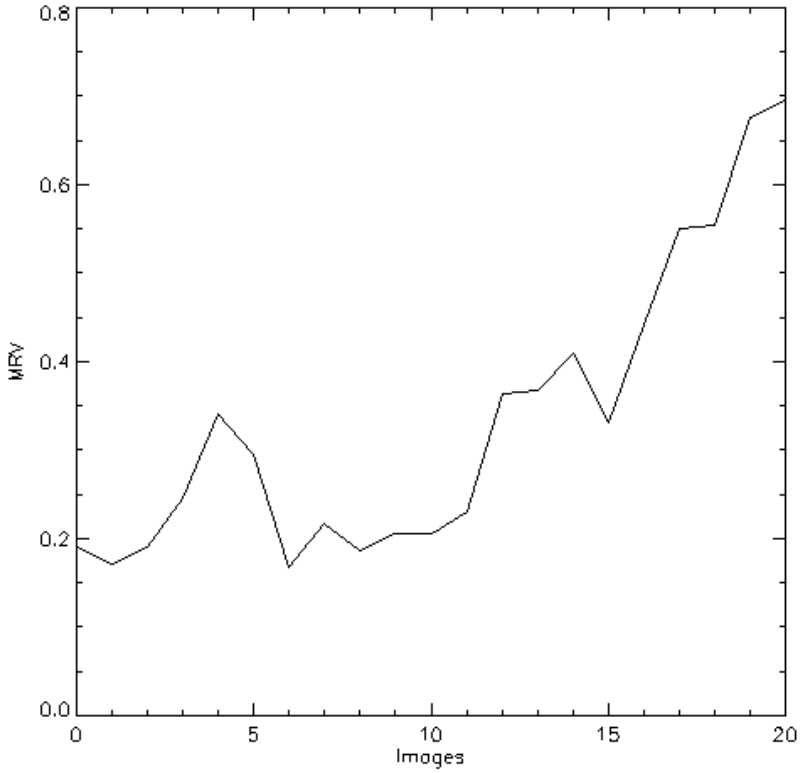

Figure 23: MRV computed for images captured on 6/24/1994. Image index on ordinate corresponds to time: 0~18: 5min interval from 4:59AM to 6:29AM, 19=8:29AM, 20=5:29PM

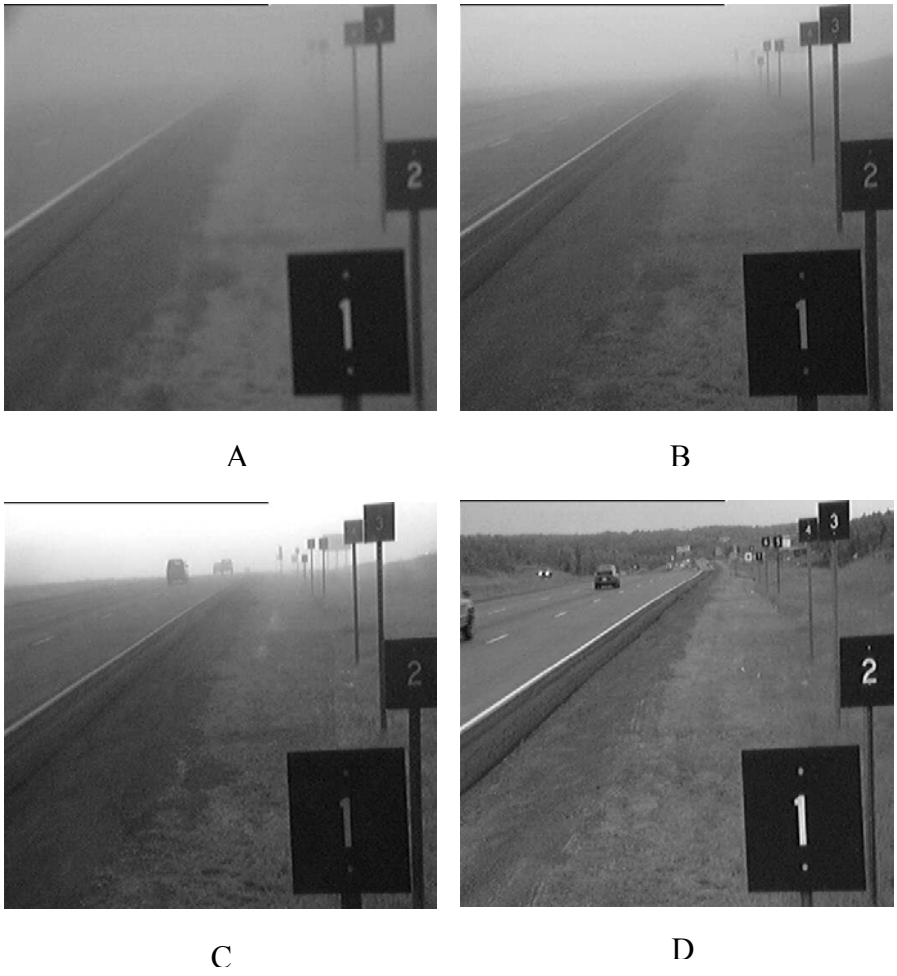

Figure 24: Sample images with MRV from Figure 23. A: MRV=17.2%, B: MRV=36.4%, C: MRV= 55.0%, D: MRV=69.6%

The next example involves 1,667 JPEG images (640x480 color) taken using a patrol vehicle on a snowy day. This example illustrates a mobile application of MVI from which a low RV section can be identified. Figure 25 shows a graph of three MVI components computed from the video images. Notice that average contrasts have an inverse relation to average luminance. On the other hand, the clarity indicator is closely correlated to average contrast. Using these three components and the control functions defined in Eq. (39)-(41), MRV was computed and plotted in Figure 26. Notice that images between 900 and 1200 show poor visibility conditions and the visibility conditions became close to a clear condition from images 1,400 to 1,600. To show images of a different percentage of MRV, Figure 27 shows images with MRV computed

as 36% and 96%. Two images were selected from the pool of 1,667 images. The differences of visual information are clearly noticeable showing reduction of visibility. This example demonstrates that MRV can even be used for a mobile condition where measurements of visual conditions independent of locations are desired.

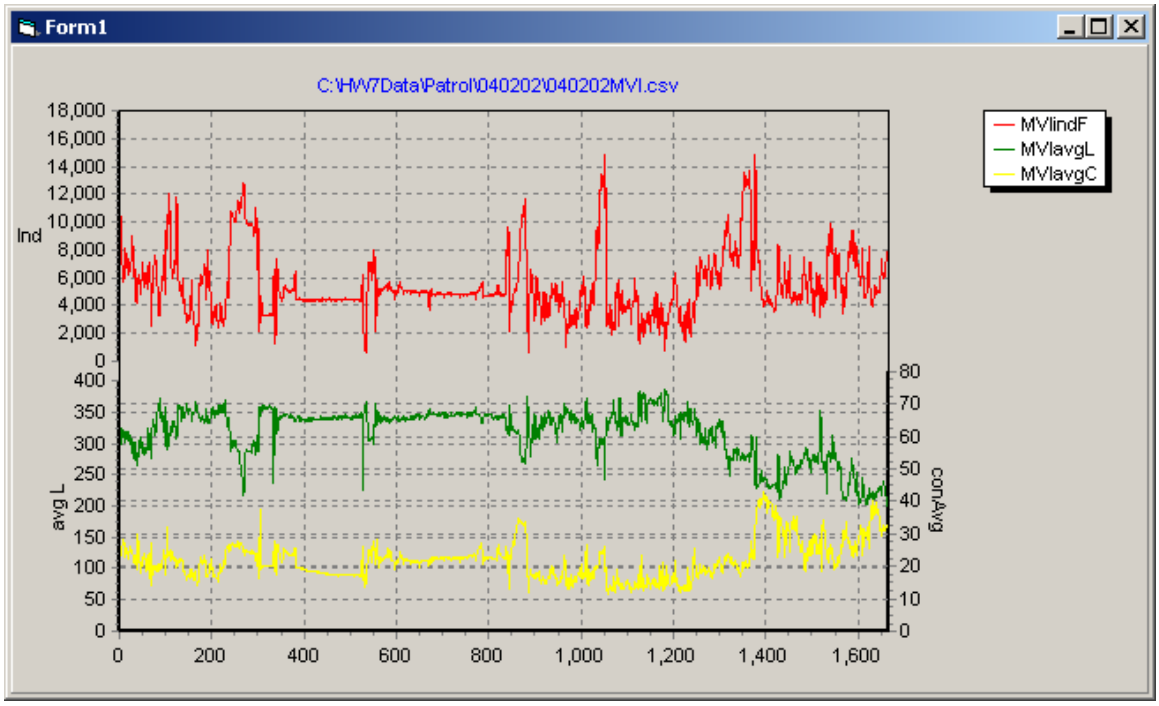

Figure 25: Plot of MVI components measured from 1,667 JPEG images. Notations used: MVIindF is I_f, MVIavgL is L_{av}, and MVIavgC is C_{av}. Horizontal axis represents image index.

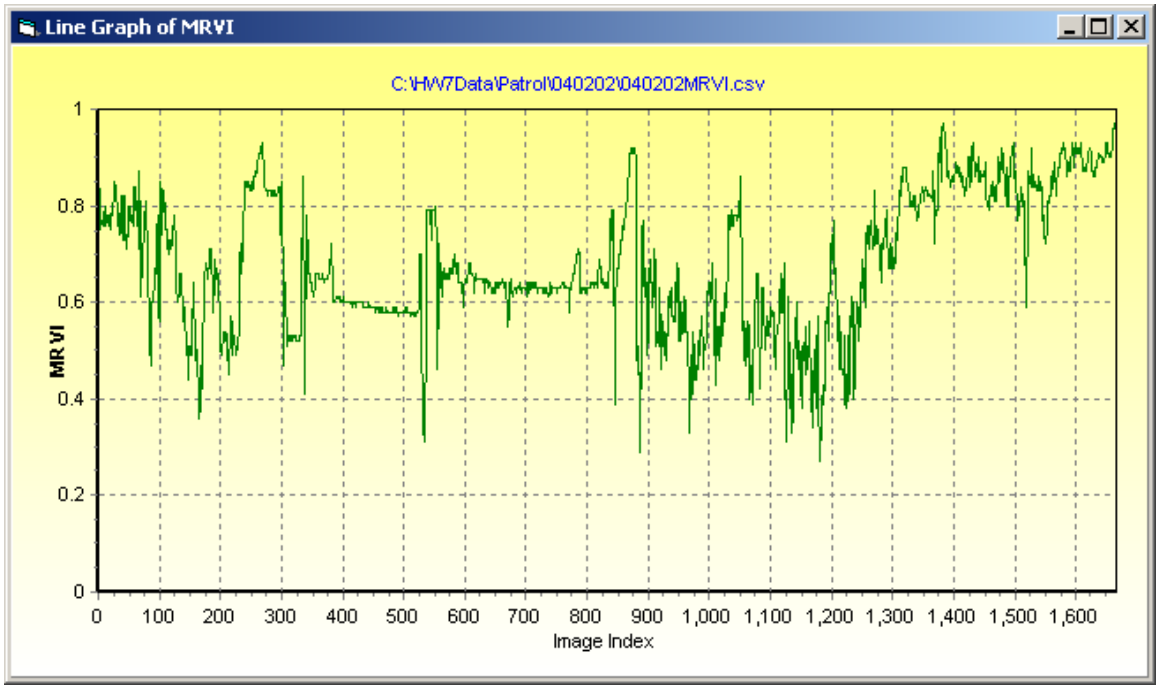

Figure 26: MRV plot using the components shown in Figure 22.

Figure 27: Left image: MRV=36%, Right image: MRV=96%

Chapter 6: Conclusion

This report presented the results of a two-year research on visibility measurements based on video cameras and image processing. It was shown that images directly obtained from common CCD video cameras have limited resolution and accuracy in capturing luminance of visual information. The second limitation of video cameras was loss of 3-D information, i.e., loss of distance information. These limitations were overcome by placing multiple targets at varying distances with a uniform contrast. It was theoretically shown and verified using real examples that visibility measurement range and accuracy increase as more targets at varying distances are available. In essence, by introducing known multiple targets the loss of distance information and limited luminance resolution in video imaging was effectively restored by inducing spatial information.

For night visibility, various apparatuses of NIR light source and camera were studied. It was found through numerous experiments and sampled data that NIR source-reflected target provides the most reliable measurements of night visibility. This approach essentially measures the opacity between the target and camera but uses an indirectly scattered light source. To increase the accuracy of this measurement method, it is recommended that an NIR band-pass filter be mounted on the NIR camera and a more uniform fine-grained reflector pattern be used as the target.

The research was further extended to develop a new concept of relative measurements of visibility. Introduction of this concept was motivated by discrepancies that are often found between the absolute measurements by today's visibility meters and what human observers see. In addition, absolute measurements of atmospheric parameters are not an effective representation of spatially variant visibility conditions. It was found that a better way of characterizing visibility conditions is using visible information that is available to motorists. An effective way of expressing visible information was a relative measurement against the visual information of an optimal weather condition, from which the relative measurement was referred to as a relative visibility.

As a measurement of visible information, three components that can be extracted from video images were mathematically derived. They are the amount of recognizable objects in the surrounding area, average luminance, and acuity of objects measured by contrast in the image. One of the difficulties of measuring human perceived visibility is that visibility is not only affected by the air particles in the atmosphere but it is also affected by air lights and objects that are available as guides to motorists. Relative visibility solves the affect of these and atmospheric parameters by directly measuring the relative amount of visual information from video images.

This research merely introduced the basic RV concept and demonstrated the measurement approaches using video images. Therefore, much research still needs to be done in the area of quantifying human perception against RV and improving the accuracy of RV computations. In order to closely simulate the human eye, future study should also include measurements of RV using stereoscopic vision systems. Another important future study would be to develop a mathematical model for computing a safe speed limit and vehicle spacing using RV.

REFERENCES

1. American Meteorological Society, *Glossary of Meteorology*, 1989.
2. W.E. Knowles Middleton, *Vision Through Atmosphere*, University of Toronto Press, 1968.
3. C.A. Douglas and R.L. Booker, *Visual Range: Concepts, Instrumental Determination and Aviation Applications*, U.S. Department of Transportation, Systems Research and Developments Service, Washington D.C. 20590, Report No. FAA-RD-77-8, 1977.
4. Duntley, S. Q., The Reduction of Contrasts by the Atmosphere," *JOSA*, vol. 38, pp. 179-191, 1948.
5. National Weather Service, *Federal Meteorological Handbook No.1*, December 1995 (also accessible through web from http://205.156.54.206/oso/oso1/oso12/fmh1.htm).
6. M. Takeuchi, "Vertical Profile and Horizontal Increase of Drift Snow Transport," *Journal of Glaciology*, vol. 26, No. 94, pp. 481-492, 1980.
7. R.A. Schmidt, "Measuring Visibility in Blowing Snow," *Proc. 2nd International Symposium on Snow Removal and Ice Control Research*, Spec. Rep. 185, pp. 200-207, May 15-19, 1978.
8. R.D. Tabler, "Using Visual Range Data for Highway Operations in Blowing Snow," *Optical Engineering*, vol. 23, No. 1, pp 55-61, 1984.
9. E. J. McCartney, *Optics of the Atmosphere: Scattering by Molecules and Particles*, John Wiley & Sons, New York, 1976.
10. Biral, "Operation and Maintenance Manual for the VPF-700 Series of Sensors," Biral HSS Sensors, UK, 1997.
11. T.M. Kwon, *An Automatic Visibility Measurement System Based on Video Cameras*, Minnesota Department of Transportation, MN/RC-1998-25, Sep. 1998.
12. Castle Rock Consultants, *Environmental Sensor Systems for Safe Traffic Operations*, U.S. Department of Transportation, Federal Highway Administration, Research and Development, Turner-Fairbank Highway Research Center, Publication No. FHWA-RD-95-073, 1995
13. Roy Hall, *Illumination and Color in Computer Generated Images*, Springer-Verlag, New York, 1988.
14. R.W.G. Hunt, *Measuring Color*, John Wiley and Sons, New York, 1987.
15. G.W. Mayer, "Wavelength Selection for Synthetic Image Generation," *Computer Vision, Graphics, and Image Processing*, vol. 41, pp. 57-79.
16. R.C. Gonzalez and R.E. Woods, *Digital Image Processing*, Addison-Wesley Publishing Company, Reading, Massachusetts, 1993.
17. E.L. Hall, *Computer Image Processing and Recognition*, Academic Press, London, UK, 1979.
18. A. Papoulis, *Probability, Random Variables, and Stochastic Process, 2nd Ed.,* McGraw-Hill, New York, 1984.